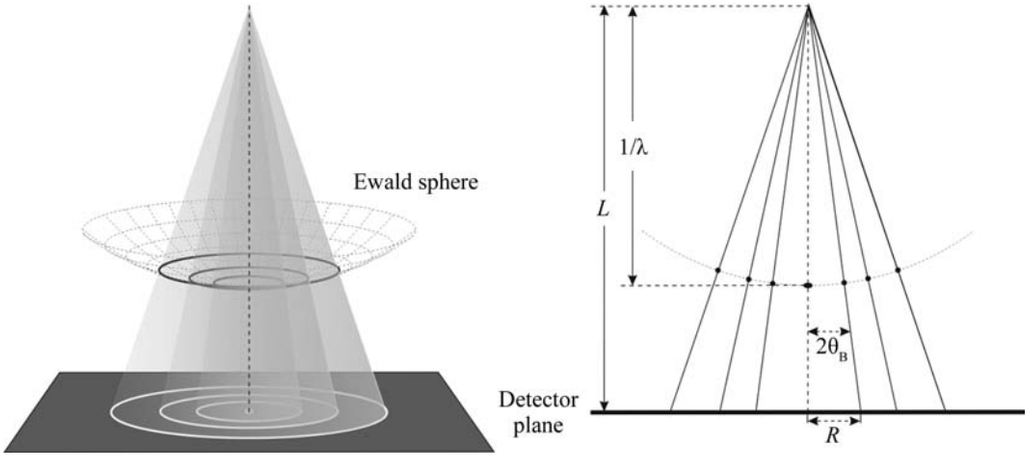

Figure 2.4.2
Schematic diagram of the Ewald sphere construction and the geometry for recording electron diffraction patterns.

development in time-resolved electron diffraction at a time resolution approaching femtoseconds (Elsayedali & Herman, 1990; Siwick *et al.*, 2003) will significantly improve the ability to interrogate structures at high spatial and time resolution.

Irradiation of both organic and inorganic materials with an electron beam can cause severe modification of the structure. The amount of energy deposited into the material can be estimated through the ratio of the elastic and inelastic scattering cross sections. For carbon the ratio for electrons (300 keV) and X-rays (with a wavelength of less than 1 Å) is comparable, meaning that the radiation damage caused by these sources is on the same scale (Henderson, 1995). Electron radiation damage is caused by all kinds of ionization processes, including bond breakdown and subsequent recombination of radicals and active molecular species. Inorganic materials can show knock-on damage (atomic displacement) or sputtering effects (loss of atoms). This damage may lead to a total structural collapse. The collective damage due to electron radiation is quantified using the electron dose and electron dose rates. In many cases the damage can be reduced by minimizing the electron dose received by the sample, cryo-protection, or deposition of a protective conductive layer (Reimer & Kohl, 2008).

This chapter covers the practical issues and theory of electron powder diffraction as well as applications for material analysis. A fundamental description of electron diffraction can be found in *International Tables for Crystallography*, Vol. C (2004) and the book by Zuo & Spence (2017). The present chapter is subdivided into seven sections. Sections 2.4.2 and 2.4.3 cover the theory and the experimental setup of an electron powder diffraction experiment using transmission electron microscopes, respectively. Sections 2.4.4 and 2.4.5 discuss the application of electron powder diffraction data to phase and texture analysis and related techniques. Rietveld refinement with electron powder diffraction data is a relatively new field; this is discussed in Section 2.4.6. The last section reviews pair distribution function (PDF) analysis using electron diffraction data.

2.4.2. Electron powder diffraction pattern geometry and intensity

By J.-M. Zuo and J. L. Lábár

The powder diffraction rings in transmission geometry appear where the cone of diffracted electron beams intersects the Ewald sphere. The intersection creates a ring of diffracted beams, which is then projected onto the planar detector (see Fig. 2.4.2) with a radius (R) according to

$$R = L \tan 2\theta_{\rm B}. \tag{2.4.1}$$

Here $\theta_{\rm B}$ is the Bragg diffraction angle and L is the camera length.

The d-spacing can be obtained by measuring the length of R in an experimental diffraction pattern using

$$d = \frac{\lambda}{2 \sin \theta_{\rm B}}. \tag{2.4.2}$$

The electron wavelength is determined by the electron accelerating voltage (Φ), in volts:

$$\lambda = \frac{h}{(2m_e\Phi)^{1/2}} \simeq \frac{1.226}{[\Phi(1 + 0.97845 \times 10^{-6}\Phi)]^{1/2}}. \tag{2.4.3}$$

The wavelength of high-energy electrons is relatively short. For 200 kV electrons, the wavelength is 0.025 Å and the Bragg angle is very small. For example, for d = 2.5 Å the electron scattering angle θ is 5 mrad. For a small Bragg angle one can use the approximation $\sin\theta \simeq \tan\theta \simeq \theta$. This gives the relationship

$$d \simeq \frac{L\lambda}{Rd}. \tag{2.4.4}$$

At large scattering angles with $\sin\theta/\lambda$ 2 Å^{-1} or greater, a better approximation is given by (Cowley & Hewat, 2004)

$$d \simeq \frac{L\lambda}{R}\left(1 + \frac{3R^2}{8L^2}\right). \tag{2.4.5}$$

The camera length L can be determined using a sample with known d-spacings, while the electron wavelength or acceleration voltage can be calibrated using high-order Laue zone (HOLZ) lines in convergent-beam electron diffraction (CBED) patterns (Zuo, 1993).

For a small parallelepiped crystal fully illuminated by a coherent electron beam of intensity I_0, the kinematic diffraction intensity is given by

$$I_{\rm SC} = I_0 \frac{\left|F_{hkl}\right|^2}{L^2}\left\{\frac{\sin[\pi\mathbf{S}_{hkl}\cdot N_1\mathbf{a}]}{\sin[\pi\mathbf{S}_{hkl}\cdot\mathbf{a}]}\frac{\sin[\pi\mathbf{S}_{hkl}\cdot N_2\mathbf{b}]}{\sin[\pi\mathbf{S}_{hkl}\cdot\mathbf{b}]}\frac{\sin[\pi\mathbf{S}_{hkl}\cdot N_3\mathbf{c}]}{\sin[\pi\mathbf{S}_{hkl}\cdot\mathbf{c}]}\right\}^2, \tag{2.4.6}$$

where N_1, N_2 and N_3 are the number of unit cells along the three axis directions, and F_{hkl} is the electron structure factor of the hkl reflection:

$$F_{hkl} = \sum_{i=1}^{n} f_i^e T_i \exp[2\pi i(hx_i + ky_i + lz_i)]. \qquad (2.4.7)$$

Here T is the atomic displacement factor, which accounts for atomic thermal vibrations, and the electron atomic scattering factor f_i^e is defined by equation (4.3.1.13) in *International Tables for Crystallography*, Vol. C (2004). For a reflection with the scattering vector $\mathbf{g}_{hkl}$ the deviation from the Bragg condition of the *hkl* reflection is expressed by the excitation error $\mathbf{S}_{hkl}$:

$$\mathbf{k} - \mathbf{k}_0 = \mathbf{g}_{hkl} + \mathbf{S}_{hkl}. \qquad (2.4.8)$$

The diffraction intensity recorded in a powder diffraction pattern is the integrated intensity over the crystal orientation and the detector area. A change in crystal orientation leads to a change in the excitation error normal to the diffracted beam in the plane of Bragg reflection. The integration in these three directions is equivalent to integration over the reciprocal-space volume around the Bragg peak. The result gives the diffraction power of a sample with a large number of crystallites for the *hkl* reflection as (Warren, 1990)

$$P_{hkl} = I_0 \frac{\lambda^2 m_{hkl} V_{\text{sample}} d_{hkl}}{2V_c^2} |F_{hkl}|^2, \qquad (2.4.9)$$

where V_{sample} is the sample volume, m_{hkl} is the multiplicity of the reflection based on the symmetry-equivalent number of *hkl* reflections, and V_c is the volume of the unit cell. For randomly oriented powder samples, the diffraction power is uniformly distributed over the bottom edge of a cone of half apex angle $2\theta_{hkl}$ and height L, and the peak intensity is more appropriately described by the power per unit length of the diffraction circle (Vainshtein, 1964):

$$I_k = \frac{P_{hkl}}{2\pi L \sin 2\theta_{hkl}} = \frac{I_0}{4\pi L} \frac{\lambda d_{hkl}^2 m_{hkl} V_{\text{sample}}}{V_c^2 \cos\theta_{hkl}} |F_{hkl}|^2. \qquad (2.4.10)$$

Here $\cos\theta_{hkl} \simeq 1$ is a good approximation for electron diffraction and this formula is presented in equation (2.4.1.3) in *International Tables for Crystallography*, Vol. C (2004).

The kinematic approximation in electron diffraction is valid only for very small crystals. Defining the validity of the kinematic approximation for different crystals has been difficult and the subject of extensive debate (Blackman, 1939; Vainshtein, 1964; Turner & Cowley, 1969; Cowley, 1995). For single-crystal electron diffraction, numerous studies using CBED have demonstrated an almost perfect fit to experimental diffraction intensities using dynamic theory. Using this fitting approach, experimental structure-factor amplitudes and phases can be measured through a refinement process with high accuracy (Saunders *et al.*, 1995; Tsuda *et al.*, 2002; Zuo, 2004). However, this approach requires knowledge of the approximate crystal structure and can rarely be used for powder electron diffraction, where unknown crystal structures are often studied. In developing a theory for the integrated intensity for powder electron diffraction, the magnitude of the dynamic effect and its dependence on crystal orientations, defects, thickness variations and crystal shape must be considered. In X-ray and neutron diffraction, the combination of these factors led to the highly successful kinematical theory of ideal imperfect crystals with randomly distributed mosaic blocks. For electron diffraction, an all-encompassing theory of integrated intensity has been elusive because of the small electron coherence length, which is much less than the size of typical mosaic blocks detected by X-ray and neutron diffraction, and strong scattering. An approximation has been developed to take account of dynamical scattering using the two-beam theory (Blackman, 1939). Under this approximation, the integrated dynamic intensity I_d over a large range of excitation is given by the expression

$$I_d \propto |F_{hkl}| \int_0^{A_{hkl}} J_0(2x)\,\mathrm{d}x. \qquad (2.4.11)$$

Here

$$A_{hkl} = \frac{\lambda\gamma|F_{hkl}|t}{V_c \cos\theta_{hkl}} \simeq \frac{\lambda\gamma|F_{hkl}|t}{V_c}, \qquad (2.4.12)$$

where t is the thickness of the crystallite along the electron-beam direction, γ is the relativistic constant of electrons and $J_0(2x)$ is the zero-order Bessel function. For a very small value of A_{hkl} the Bessel function $J_0(2x)$ is nearly constant with a value of 1 and the diffraction intensity approaches that of the kinematical limit. From this, the following formula can be derived for the dynamical intensity:

$$I_d = \frac{I_0}{4\pi L} \frac{d_{hkl}^2 m_{hkl} V_{\text{sample}}}{V_c \gamma t} |F_{hkl}| \int_0^{A_{hkl}} J_0(2x)\,\mathrm{d}x. \qquad (2.4.13)$$

For very large A_{hkl}, the integral over the Bessel function approaches the value of 1/2 and in this case the diffraction intensity is proportional to the structure-factor amplitude instead of its square as predicted by kinematical theory.

The extent of dynamic effects that can be reduced by averaging over crystal orientations has been demonstrated by precession electron diffraction (PED). This technique was originally developed by Vincent & Midgley (1994) to improve the single-crystal electron diffraction intensities for structural analysis. In PED, the incident electron beam is tilted and precessed along a conical surface that is centred on the electron optical axis. Below the crystal, the diffraction pattern is tilted back with the position of the direct beam remaining approximately constant during precession. The diffraction pattern then generally appears similar to a conventional electron diffraction pattern. The measured diffraction intensity, however, is a double integration over the two-dimensional detector and the incident-beam angles defined by the precession cone surface. Experimental and theoretical studies of PED integrated intensities have shown an overall 'more kinematical' behaviour with less sensitivity to crystal thickness and exact orientation than for conventional electron diffraction patterns. Simulations also showed that the dynamical effects are still present in the PED integrated intensities, but the extent of the dynamic effect as measured by the correlation between the integrated intensity and the squared amplitude of the structure factor follows the empirical rules:

(i) The correlation increases with the precession angle.
(ii) The correlation is more pronounced for higher-order reflections than lower-order ones, for which the integration over the different excitation error is less complete.
(iii) The correlation also improves as the crystal thickness decreases.

In the electron powder diffraction of randomly oriented crystals, the angular integration is performed over the entire solid angle. Zone-axis patterns with enhanced dynamical interaction between the diffracted beams are also included in this solid angle. However, the overall probability for a crystal to be in exact zone-axis orientation is very small, even if the zone axis is defined